SEGMENTAL CABLE EVALUATION OF SOMATIC TRANSIENTS IN HIPPOCAMPAL NEURONS (CA1, CA3, AND DENTATE)

DENNIS A. TURNER
Institute of Neurophysiology, University of Oslo, Oslo 1, Norway

ABSTRACT This study describes a detailed cable model of neuronal structure, which can predict the effects of discrete transient inputs. Neurons in in vitro hippocampal slices (CA1 and CA3 pyramidal cells and dentate granule neurons; $n = 4$ each) were physiologically characterized and stained with horseradish peroxidase (HRP). The HRP morphology was approximated with numerous small segments. The cable model included both these segments and spatially dispersed dendritic spines. The transient response function at the soma of the segmental model was numerically derived, and charging responses to simulated current inputs were computed. These simulations were compared with the physiological charging responses from the somatic penetrations, using an analysis of the charging time constants (τ_i) and intercepts. The time constant ratio (τ_0/τ_1) did not significantly differ between the observed and simulated responses. A second index of comparison was the equivalent cylinder electrotonic length (L), which was derived using only the τ_i values and their intercepts. The L values also did not differ significantly between the observed and simulated transients and averaged 0.91 length constant. Thus, using criteria based only on analysis of charging responses, the segmental cable model recreated accurately the observed transients at the soma. The equivalent cylinder model (with a lumped soma) could also adequately simulate the observed somatic transients, using the same criteria. However, the hippocampal neurons (particularly the pyramidal cells) did not appear to satisfy the equivalent cylinder assumption anatomically. Thus, the analysis of somatic charging transients alone may not be sufficient to discriminate between the two models of hippocampal neurons. Anatomical evidence indicates that, particularly for discrete dendritic inputs, the detailed segmental model may be more appropriate than the equivalent cylinder model.

INTRODUCTION

Excitatory inputs to pyramidal and granule cells in the hippocampus synapse mainly onto dendritic spines (Andersen et al., 1980; Fifkova and Anderson, 1981; Fifkova and Van Harreveld, 1977; Lee et al., 1980; Minkwitz, 1976; Scheibel and Scheibel, 1968). However, dendritic regions have been relatively inaccessible to direct physiological investigation. Thus, information regarding excitatory inputs has mainly been inferred from somatic recordings (Andersen et al., 1980; Barnes and McNaughton, 1980; Johnston and Brown, 1983; Turner and Schwartzkroin, 1980, 1983). Such indirect information has left unanswered the role of both dendrites and dendritic spines in the processing and transfer of synaptic signals in the hippocampus.

Dendritic neuron models have been applied to hippocampal neurons to define both the nature of synaptic processing in neurons and the effect of dendritic branching on the interpretation of somatic recordings (Brown et al., 1981*a*; Durand et al., 1983; Johnston, 1981; Traub and Llinas, 1979; Turner and Schwartzkroin, 1980, 1983). One model type is a segment-by-segment cable evaluation of dendritic branching (Koch et al., 1982; Rall, 1959; Turner and Schwartzkroin, 1980, 1983). Another model involves physiological analysis of somatic transients, which assumes the equivalent cylinder model (Brown et al., 1981*a*; Durand et al., 1983; Johnston, 1981). A third model includes the use of isopotential compartments (Traub and Llinas, 1979). Electrical parameters involved in the analysis of synaptic inputs, such as electronic length (L) and the dendrite to soma conductance ratio (ρ), have not been evaluated in similar circumstances by these models and hence are difficult to compare. Also, none of these three types of models has proved entirely satisfactory for the evaluation of single dendritic spine or shaft transients (Rall, 1974; Rinzel and Rall, 1974).

Cable analysis using both Laplace transforms and detailed dendritic structure has previously been employed in the evaluation of dendritic synaptic inputs (Barrett and Crill, 1974 *a*, *b*; Koch et al., 1982; Norman, 1972; Rinzel and Rall, 1974). With this model, a transient response function can be calculated that is equivalent to the effective input impedance at any site. In addition, using a segment-by-segment dendritic approximation, voltage or current transfer from an input site to other arbitrary anatomical locations can be numerically evaluated. This powerful approach allows the comparison of an observed

physiological input (such as to the soma) with model predictions for the same site.

This report presents an analysis of somatic responses in three major classes of hippocampal cells. These neurons have been examined physiologically and then stained intracellularly with horseradish peroxidase (HRP) (Durand et al., 1983; Turner and Schwartzkroin, 1980, 1983). The HRP morphology has been approximated by a series of segments, which were used in a transient cable analysis. One aim of this evaluation is to compare the segmental model predictions with physiological observations on the same neuron. Time constant analysis is used as an index of comparison (Brown et al., 1981*a*; Durand et al., 1983; Johnston, 1981; Rall, 1969). There is a good correlation between the observed transients and the responses derived by analysis of the detailed anatomical structure. The following study (Turner, 1984) uses the same format of segmental cable calculations for an analysis of transient dendritic spine inputs. An abstract of this work has been published (Turner, 1982).

METHODS

Experimental Techniques

The cells included in this analysis represent a subset ($n = 12$) of those reported previously (Turner and Schwartzkroin, 1980, 1983). All neurons were studied in guinea pig hippocampal slices, 400–450 μm thick, maintained in vitro at 37°C (Schwartzkroin, 1975). The glass microelectrodes were filled with a solution consisting of 4% horseradish peroxidase (HRP; Type VI, Sigma Chemical Co., St. Louis, MO) in 0.2 M KCl, buffered to pH 8.6 with Tris (Sigma Chemical Co). The intracellular electrodes were selected to have a resistance (at 30 Hz) of 110–125 MΩ. At this resistance, the electrodes were able to pass up to 1 nA of current, in either the depolarizing or hyperpolarizing direction, without rectification. All electrodes used for analysis could be adequately balanced at both the onset and termination of current injection. Thus, except for the higher resistance, these HRP electrodes demonstrated acceptable characteristics.

Minimal requirements for acceptable intracellular records included a resting potential of at least 55 mV, a spike height of 60 mV, regular repetitive firing to depolarizing pulses, and an intact response to orthodromic synaptic stimulation. Physiological analysis included the estimation of neuron input resistance (R_N) and charging time constants (τ_i). These cells demonstrated nonlinearities to both large hyperpolarizing and depolarizing currents, so analysis was limited to small hyperpolarizing current pulses (0.1–0.5 nA). R_N was estimated from the slope (using least-squares regression) of a current-voltage plot, constructed from the steady state voltage response to constant current steps (Fig. 3 *B*). Time constant analysis could not be reliably performed using differentiated voltage traces, because of the high resistance of the electrodes. Instead, the normalized charging function $1 - V/V_f$ (Wong and Prince, 1981) was plotted on semilogarithmic coordinates vs. time (Fig. 3 *A*). Two time constants could be extracted in the physiological charging transients, using a "peeling" method (Rall, 1969) and exponential least-squares regression analysis. For both the R_N and τ_i plots, the standard deviation (SD) of the slope was calculated, as well as a 95% confidence interval for the regression lines (Fig. 3, *A* and *B*).

After physiological evaluation, HRP was iontophoresed into the neuron. Immediately after the injection, the slice was fixed with 1.25% glutaraldehyde and 1% formaldehyde in a phosphate buffer (pH 7.6). Slice sections (75 μm) were serially exposed to 0.5% $CoCl_2$ (in Tris buffer at pH 7.6) and 0.01% H_2O_2 plus 0.05% diaminobenzidine (in phosphate buffer at pH 7.6). Linear shrinkage estimates (from fresh tissue through the processing) averaged 4.0% (Turner and Schwartzkroin, 1983). Subsequent dimensions were corrected for this shrinkage factor. The stained neurons were drawn at 1,500× under oil immersion, using a camera lucida attachment (Fig. 4). The vertical dimensions were measured between branch points and adjusted for the refractive index using Snell's law.

The somatic profile was approximated as a more or less regular geometric body. The anatomic boundary of the soma was determined to be at an arbitrary point where the taper into the major dendritic processes ended. The dendritic tree was divided into a number of smooth cylindrical segments. There was at least one segment, and often more, between each branch point. Branch diameter changes were approximated by increasing the number of segments, to a tolerance of 10%. The total count of cylindrical segments per neuron varied, ranging from 200 to 300 for the dentate granule neurons to >1,000 for many of the CA1 pyramidal cells. A complete map of each neuron required only the length and diameter of each segment, as well as its interconnection to the other segments.

Time Constant Analysis

The physiologically observed somatic responses to a hyperpolarizing step input were filmed and enlarged (Fig. 3 *A*). The neuron's charging response was assumed to be a sum of exponentials (Rall, 1969):

$$V_f - V = C_0 e^{-t/\tau_0} + C_1 e^{-t/\tau_1} + C_2 e^{-t/\tau_2} + \dots \quad (1)$$

V represents the change in membrane potential from the resting potential, V_f is the final steady state potential reached after full equilibration, and the c values are coefficients. To enhance the smaller coefficients, the charging response was divided by V_f (Wong and Prince, 1981):

$$1 - \frac{V}{V_f} = \frac{C_0}{V_f} e^{-t/\tau_0} + \frac{C_1}{V_f} e^{-t/\tau_1} + \dots \quad (2)$$

The time constants (τ_0, τ_1) and intercepts ($y_i = C_i/V_f$) were used to estimate the dendrite to soma conductance ratio (ρ) and the terminating electrotonic length (L). These values were calculated for the comparison of the observed and simulated transients, as well as comparison with previous reports regarding hippocampal neurons (Brown et al., 1981*a*; Durand et al., 1983; Johnston, 1981). Thus, ρ was first estimated using Eq. 3 of Brown et al. (1981*a*):

$$\rho = \frac{\tau_0}{V_f}\left(\frac{C_0}{\tau_0} + \frac{C_1}{\tau_1}\right) - 1 = y_0 + \frac{\tau_0}{\tau_1} y_1 - 1, \quad (3)$$

substituting the y_i for the first two terms. Using this ρ value, an initial L value was derived using Rall's approximation (1969):

$$L = \left[\frac{\rho/(\rho + 1)}{(\tau_0/\tau_1) - 1}\right]^{1/2} \quad (4)$$

A more exact value for L was then calculated, substituting the approximate L value from Eq. 4 into the following equation (Rall, 1969):

$$\rho + \propto \cot(\propto L) \tanh(L) = 0;$$
$$\propto = (\tau_0/\tau_1 - 1)^{1/2}. \quad (5)$$

The L value was iteratively corrected until the equation was satisfied. Similar values were also calculated for the simulated transients.

Cable Calculations

The cylindrical segments from the dendritic reconstructions were considered to be short pieces of core-conducting cable, which connected at branch points (Fig. 1). Each segment was characterized by a geometric length (l) and a uniform diameter (d). Somatic current inputs were evaluated as a current source with zero internal admittance (or infinite

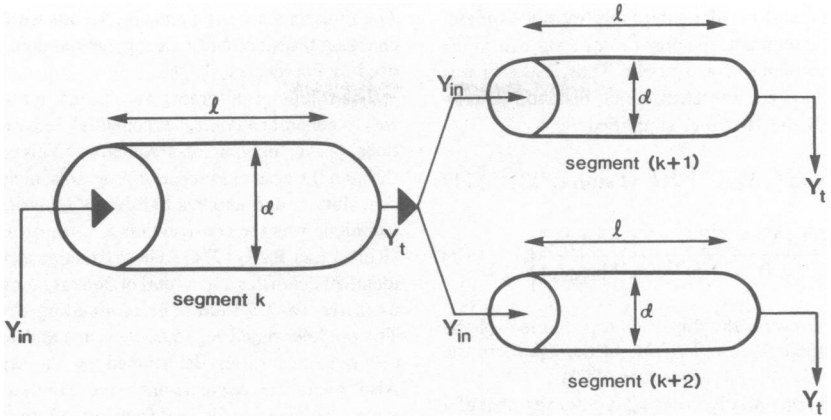

FIGURE 1 A schematic of a single branch point in the segmental cable model. Each cylinder depicts a cable segment derived from neuronal measurements. Each segment possessed a geometric length (l) and diameter (d). First, the length constants (λ) of the daughter branches ($k + 1$ and $k + 2$) were calculated. Second, the geometric lengths were normalized by the length constant to derive the electrotonic lengths. Third, the input admittances Y_{in} $(k + 1)$ and Y_{in} $(k + 2)$ were calculated and then summed. This sum, after normalization, formed the terminating admittance of the parent branch $[\tilde{Y}_t^*(k)]$. In the next iteration, the kth branch shown was one of the daughter branches, and so on, until the soma junction was reached. Since this was a unidirectional analysis, the arrows show the direction of current flow, from the soma (proximal, to the left) toward the dendritic terminations (distal, to the right).

impedance) at the proximal terminus of each segment (toward the left in Fig. 1). The distal end of any segment possessed no electrical sources. The equations presented below are consistent with the terminology and Laplace cable approach presented by Barrett and Crill (1974 *a*), Koch et al. (1982), Norman (1972), and Rinzel and Rall (1974). Laplace transformed variables are expressed with a tilde (~).

The assumptions involved in the transformation of a geometric dendritic tree into an array of cable segments have been discussed by Rall (1959), Barrett and Crill (1974 *a*), and Turner and Schwartzkroin (1980, 1983). These assumptions are:

(*a*) The membrane of the cable segments and the soma is assumed to be passive and uniform, and it consists of parallel resistive and capacitative elements.

(*b*) The extracellular space is assumed to have infinite conductivity. This assumption excludes the external resistivity and the specific geometry of dendrites and branch angles.

(*c*) The soma is considered to be a single, lumped isopotential region, which joins the major dendritic trunks.

(*d*) There is continuity of current and voltage at branch points and the soma-dendritic junction, which implies that the membrane surface is continuous.

The validity of these assumptions has also been discussed by Rall (1959, 1977). The major independent variables in this analysis were:

(*a*) The specific internal resistivity (R_i) was assigned a value of 75 Ω·cm. This is the midpoint of values assumed in other analyses (Durand et al., 1983; Lux and Schubert, 1975; Rall, 1959, 1977; Turner and Schwartzkroin, 1980, 1983) and is close to the value of 70 Ω·cm measured by Barrett and Crill (1974 *a*).

(*b*) The normalized terminating admittance ($\tilde{Y}_t^*$) of the most distal segments was assumed to be either 0 (a "sealed-end" termination) or 1 (an infinite cable termination). These two values represented the extremes enclosing the probable "real" value.

(*c*) The value for angular frequency ($\omega\tau = 2\pi f\tau$) was varied from 1.0×10^{-1} to 1.0×10^{5}. The frequencies were normalized for the time constant of the membrane. Thus, a specific time constant value was not required, and the results are presented in terms of normalized time ($T = t/\tau$).

For any particular set of the two independent variables, R_i and $\tilde{Y}_t^*$, a unique value for specific membrane resistivity (R_m) was derived ($\omega\tau = 0$). An initial value for R_m was first assumed and then progressively corrected until the calculated value of R_N was within 0.1% of the observed R_N value. This R_m value was a constant for that cell for the remainder of the calculations. The somatic input impedance ($\tilde{Z}_N$) was calculated at each frequency (1,000 $\omega\tau$ values were used), and linear interpolation of $\tilde{Z}_N$ between any two frequencies resulted in an error of <0.1%.

After Laplace transformation, the general cable equations can be expressed as (Norman, 1972):

$$\frac{d^2\,\tilde{V}(x,s)}{dx} = \frac{q^2}{\lambda^2}\,\tilde{V}(x,s); \tag{6}$$

$$\tilde{I}(x,s) = \frac{1}{r_i}\,\frac{d\,\tilde{V}(x,s)}{dx}. \tag{7}$$

$\tilde{V}(x, s)$, the Laplace transform of the voltage, is a function of x (geometric distance along the cable) and s. Here, s is a dimensionless, normalized frequency ($s = j\omega\tau$) and $q = (1 + s)^{1/2}$. $\tilde{I}(x, s)$ is the Laplace transform of the longitudinal current in the cable, $\lambda = [(d\,R_m)/(4R_i)]^{1/2}$ is the length constant for the segment, and r_i is the overall internal resistivity.

The solutions to Eqs. 6 and 7 can be expressed in terms of hyperbolic sine (sinh) and cosine (cosh), as in Rall (1959):

$$\tilde{V}(x,s)/\tilde{V}(l,s) = \cosh[q(l-x)/\lambda] + \tilde{Y}_t^*(l,s)\sinh[q(l-x)/\lambda]; \tag{8}$$

$$\tilde{I}(x,s)/\tilde{V}(l,s) = \frac{q}{r_i\lambda}\{\sinh[q(l-x)/\lambda] + \tilde{Y}_t^*(l,s)\cosh[q(l-x)/\lambda]\}. \tag{9}$$

l is the geometric length of the cable segment, x is the geometric position along the cable, and $\tilde{Y}_t^*$ is the normalized terminating admittance of the segment. $x = 0$ is the proximal end (toward the soma) of the segment, and $x = l$ is the distal or terminating end, as depicted in Fig. 1.

The desired expression is the input admittance into the proximal end of the cable segment. This value is obtained by dividing the current solution (Eq. 9) by the voltage solution (Eq. 8):

$$\tilde{Y}_{in}(x,s) = \frac{\tilde{I}(x,s)}{\tilde{V}(x,s)} = \frac{q}{r_i\lambda} \cdot \left\{\frac{\sinh[q(l-x)/\lambda] + \tilde{Y}_t^*(l,s)\cosh[q(l-x)/\lambda]}{\cosh[q(l-x)/\lambda] + \tilde{Y}_t^*(l,s)\sinh[q(l-x)/\lambda]}\right\}. \tag{10}$$

The voltage at intermediate points (x) along the cable was not required, since there were sufficient cable segments to approximate a state in which dendritic inputs were at the terminus of a segment. Thus, $\tilde{Y}_{in}(x, s)$ was always calculated with $x = 0$. Since the electrotonic distance for any segment is $X = l/\lambda$, then Eqs. 8 and 10 can be simplified:

$$\tilde{V}(0, s)/\tilde{V}(l, s) = \cosh(qX) + \tilde{Y}_t^*(l, s) \sinh(qX); \quad (11)$$

$$\tilde{Y}(0, s) = \frac{q}{r_i\lambda}\left[\frac{\sinh(qX) + \tilde{Y}_t^*(l, s)\cosh(qX)}{\cosh(qX) + \tilde{Y}_t^*(l, s)\sinh(qX)}\right]. \quad (12)$$

The factor $q/(r_i\lambda)$ in Eq. 12 converts the dimensionless quotient of the right side into absolute admittance on the left side of the equation; the asterisk indicates a dimensionless quantity (Norman, 1972).

Eqs. 11 and 12 were applied sequentially to each daughter segment of a branch point (Fig. 1). The $\tilde{Y}_t^*$ of only the most distal segments was assumed to have a value of either 0 or 1, as discussed above. At each branch point, the absolute admittances of the daughter branches were first summed (Fig. 1). The admittance sum, once normalized, became the $\tilde{Y}_t^*$ of the parent segment, for use in the next iteration of Eq. 12. The branch point calculations proceeded proximally, one branch point at a time, until the major trunk segment of each dendrite and its junction with the soma was reached. The input admittances of the major dendrites were summed, together with that of the soma:

$$\tilde{Y}_N = \tilde{Y}_{soma} + \Sigma\,\tilde{Y}_{den} = \left[\frac{\text{soma area}}{R_m(1 + s)}\right] + \Sigma\,\tilde{Y}_{den}. \quad (13)$$

$\tilde{Y}_N$ was the total neuron admittance, the inverse of which was $\tilde{Z}_N$, the input impedance at the soma as a function of frequency.

The calculated input impedance, $\tilde{Z}_N$ (a function of frequency), was numerically inverted to Z_N (a function of time) with an inverse Fourier transform (Norman, 1972):

$$Z_N(k\Delta T) = \frac{n}{2\pi}\sum_{m=0}^{n-1} [\tilde{Z}_N(m\Delta\omega\tau)\exp(jm\,\Delta\omega\tau\, k\Delta T)]\,\Delta\omega\tau. \quad (14)$$

The time intervals for the transient response function Z_N were expressed in units of T, $T = t/\tau$. The frequency harmonics were multiples of $\Delta\omega\tau$. n was the number of points in the transform and $N\Delta T$ (the period) was either 6.4τ or 9.6τ. The base frequency was set in terms of the normalized time intervals desired: $\Delta\omega\tau = (2\pi)/(n\Delta T)$. A value of $n = 4{,}096$ was the minimum size adequate to resolve the higher components of the frequency response. For $n\Delta T = 6.4\tau$, the base frequency $\Delta\omega\tau$ was 0.98 and the maximum frequency $(n - 1)\,\Delta\omega\tau$ was 4,000.

The errors involved in this transform have been discussed by Norman (1972). These involve truncation of the spectral input (failure to consider the full frequency response) and discrete sampling of both the input frequency and the output time values. In the present calculations, the Fourier coefficients were chosen to partially correct for these errors, as discussed by Normal (1972). The largest residual error was the difficulty with spectral truncation. Even with the maximum frequency at ~4,000, the 4,096-point Fourier transform was just adequate to sample the higher frequencies for the faster decay processes (Fig. 5 *A*), while still allowing the response to decay completely. This truncation error was adjusted to <1% by increasing n to 4,096. The resulting transforms could reliably define both the single time constant of an exponential decay and the two time constants of the simulated charging transients.

A linear convolution of the soma transient response Z_N with a step current pulse I_{step} resulted in the calculated voltage response $[V(k\Delta T)]$ at the soma:

$$V(k\Delta T) = \sum_{m=0}^{n-1}\{Z_N(m\Delta T)\, I_{step}\,[(k - m)\Delta T]\}\,(\Delta T). \quad (15)$$

The time constant ratio and coefficients were derived from the simulated charging transients with an exponential decay program (Discrete), developed by Provencher (1976).

The computer programs were tested in a variety of ways. One method was to generate a control exponential decay along with the cell computations (as a function of frequency). This simple decay was analyzed through the entire sequence of programs, including the Fourier transform, convolution, and exponential decay analysis (Fig. 5 *A* and *B*). Another technique was the construction of a complex equivalent cylinder neuron (Rinzel and Rall, 1974). The particular example selected possessed six identical dendrites and a total of 366 segments. The terminating dendritic diameter was 0.20 μm. The terminating electrotonic length was 1.00λ. The predetermined R_m (5,000 Ω·cm²) and R_N (29.8 MΩ) for this model cell were accurately determined by the segmental cable calculations. Also, analytical comparisons were computed for terminal input resistance, voltage transfer, and transient solutions at the soma.

Dendritic Spine Calculations

Small dendritic spines have been observed both on pyramidal cells and dentate granule neurons in the hippocampus (Englisch et al., 1974; Fifkova and Anderson, 1981; Fifkova and Van Harreveld, 1977; Lee et al., 1980; Lorente de No, 1934; Meyer and Ferres-Torres, 1978; Minkwitz 1976; Scheibel and Scheibel, 1968; Wenzel et al., 1981; Westrum and Blackstad, 1962). Small dendritic spines were incorporated in the segmental cable model, but the large, complex, mossy fiber endings on the CA3 pyramidal cells were excluded from the analysis. Because of the small number of the mossy fiber terminals per neuron (~200), this loss of area should not be significant, especially compared with the much larger numbers of small dendritic spines (6,000–13,000 per cell) on the CA3 pyramidal cells.

Dendritic spines of CA1 pyramidal cells were studied in an electron microscopic (EM) reconstruction study (Westrum and Blackstad, 1962). These spines were found to possess average dimensions of 0.1 μm for the minimum diameter of the spine neck, 0.4 μm for the spine neck length (from the dendritic shaft to the base of the spine head), and 0.40 μm² for the surface area of the spine head (as in Fig. 2 *A*). Another report has

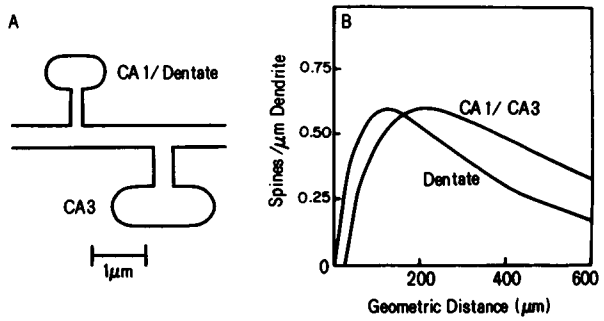

FIGURE 2 (*A*) A schematic depiction of typical dendritic spine sizes, as used in the calculations. For the CA1 and dentate neurons (to the left), the spine diameter used was 0.17 μm, the spine neck length was 0.67 μm, and the surface area of the spine head was 1.12 μm². For the CA3 pyramidal cells (to the right), the dimensions were: spine neck diameter, 0.37 μm; spine neck length, 0.70 μm; spine head surface area, 2.0 μm². The spine head was treated as a lumped admittance in the calculations. The spine neck was considered a short piece of core-conducting cable. (*B*) This plot shows spine density vs. geometric distance (Eq. 16, Methods). The CA1/CA3 distribution was constrained to have a maximum at ~200 μm. The equation is a double exponential, patterned after spine measurements by Valverde and Ruiz-Marcos (1969). The dentate plot was patterned after Golgi measurements by Wenzel et al. (1981). The maxima for both of the plots coincide with Golgi measurements for the same region.

confirmed the above minimum dimensions for CA1 stratum radiatum spines (Lee et al., 1980). The exact linear shrinkage is not known for any of these studies. Such shrinkage is thought to be in the neighborhood of 40% for typical EM preparations. However, there is also considerable variability, depending on the orientation of fiber direction, tissue type, technique of fixation, and further processing (T. Blackstad, personal communication). As an initial estimate, a linear shrinkage factor of 40% was used to correct the EM spine dimensions used in the calculations (Fig. 2). The corrected dimensions in the CA1 pyramidal cells were: spine neck diameter, 0.17 μm; spine neck length, 0.67 μm; spine head surface area, 1.12 μm^2.

The density distribution of small spines in the apical dendritic region of CA1 pyramidal cells has been reported (Englisch et al., 1974; Meyer and Ferres-Torres, 1978; Minkwitz, 1976; Wenzel et al., 1973). These studies defined constraints on the form of this spine distribution:

(*a*) Few spines occurred in the proximal 50 μm of the major apical dendrites, as measured from the cell body.

(*b*) The density of spines peaked at ~200–300 μm along the apical dendrite. This density peak has been measured to be 0.55–0.6 spines per micrometer length of dendrite.

(*c*) Minkwitz (1976) reported a sharp drop in spine density distal to 400 μm (in rats). Synaptic density measurements by Andersen et al. (1980) in the guinea pig indicated a much more gradual taper, with 70% of the peak remaining at 400 μm.

An equation to fit these requirements was patterned after the form developed by Valverde and Ruiz-Marcos (1969):

$$X_S = Y_M (1 - K e^{-B\Sigma l}) e^{-IF\Sigma l}. \quad (16)$$

Y_M, K, B, and IF are coefficients; X_S is the resulting number of spines per 50 μm of dendritic length, and Σl is the summated geometric length to a specific segment, from the soma. For the CA1 region, the requirements above were satisfied with the following parameter values (plotted in Fig. 2 *B*): $Y_M = 125$, $K = 1.10$, $B = 7.0 \times 10^{-3}$, and $IF = 2.25 \times 10^{-3}$. The density of spines along a segment was fixed for that segment by the summated length to the midpoint of the segment.

Fifkova and Anderson (1981) and Fifkova and Van Harreveld (1977) found the average minimum diameter of the spine necks of dentate granule neurons to be near that of the CA1 pyramidal cells, 0.10–0.13 μm. Because of the similarity of this dimension, the dentate spines were assumed to be identical to the CA1 spines above. Spine density has also been measured in dentate granule cells (Wenzel et al., 1981). These measurements from rat Golgi studies were adapted to the form of Eq. 16. The parameters in this case were: $Y_M = 100$, $K = 1.05$, $B = 1.5 \times 10^{-2}$, and $IF = 3.0 \times 10^{-3}$. This distribution has also been plotted in Fig. 2 *B*.

The dimensions of small dendritic spines in CA3 pyramidal cells have been reported, using EM measurements (Turner and Schwartzkroin, 1983). After correcting these values for shrinkage (40%), the final values used in the calculations were (Fig. 3): spine neck diameter, 0.37 μm; spine neck length, 0.70 μm; spine head surface area, 2.0 μm^2. The distribution of small spines has not been reported for CA3 pyramidal cells, so the CA1 pyramidal cell distribution was used in the calculations as an initial estimate.

The spine neck was considered to be a short cable segment. The spine head was evaluated as a lumped, isopotential admittance, with a value proportional to its surface area. The individual admittance into each spine neck included (through Eq. 12) the effect of the spine head, which was considered to be a terminating admittance. Each junction of spine neck and segment was treated as a separate branch junction, which required an application of Eq. 12. The spatial dispersion of spines was specifically included in the computations. Values for spine R_m and R_i were assumed to be identical to those for the remainder of the neuron.

The spine calculations required additional assumptions about the nature of the segmental cable model:

(*a*) The dendritic spines were assumed to be uniform and possess the "average" dimensions given above and in Fig. 2 *A* for each cell type.

(*b*) Although the actual EM linear shrinkage factor is unknown, it has been approximated as 40% in this initial evaluation.

(*c*) The spines were assumed to be distributed as described by Eq. 16 (plotted in Fig. 3 *B*). Although spine density has been measured only for the apical dendrites within the CA1 region, the same distribution was also assumed for the basilar dendrites (for which there are no comparable measurements available) and for the CA3 pyramidal neurons. The dentate distribution in Fig. 2 *B* was assumed to be valid only for the dentate granule neurons (see Feldman and Peters [1979] for a critique of spine density estimation).

(*d*) The dendritic spine head, like the soma, was considered to be an isopotential, lumped admittance, proportional to the surface area.

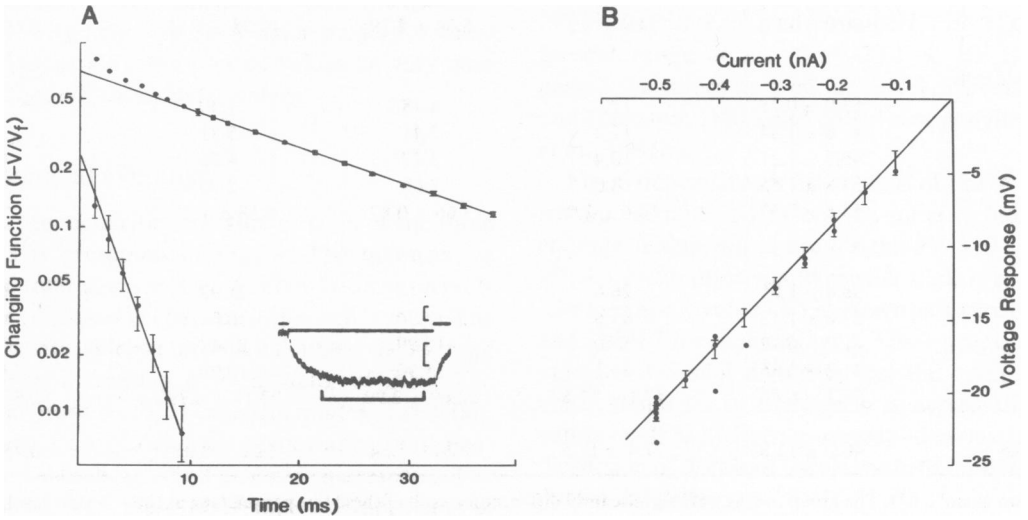

FIGURE 3 (*A*) The inset shows an intracellular injection of a 0.5-nA current pulse (hyperpolarizing) into a CA1 pyramidal cell (illustrated in Fig. 4 *A*), and the resulting voltage response. The upper trace is the current monitor. The scale indicates 10 mV and 1.0 nA in the vertical directions and 100 ms in the horizontal direction. The plot demonstrates the terminal linear decay of the charging function, and the peeling method. The τ_0 value measured 21.1 ± 0.24 ms ($r = 0.99$) and τ_1 measured 2.97 ± 0.25 ms ($r = 0.97$). (*B*) A current-voltage plot from the same cell was derived by plotting the steady state voltage (at the end of the current pulse) vs. the current injected. The line was constructed with a linear least-squares regression and indicated an R_N of 42.7 ± 0.72 MΩ ($r = 0.98$).

RESULTS

Physiological Observations

Fig. 3 *A* demonstrates a typical charging transient, in response to a step hyperpolarizing current input at the soma. Fig. 3 *B* presents a current-voltage plot from the same cell. The R_N values for the three cell classes (Table I) differed significantly ($P = 0.01$). The group averages varied from 30.0 ± 11.0 MΩ (mean ± SD) for the CA1 pyramidal cells to 53.5 ± 7.6 MΩ for the dentate granule neurons, with the CA3 pyramidal cells intermediate. The standard deviation of the slopes from the R_N regression analysis showed a very small coefficient of variation (1.5%; Table I). Thus, most of the variance of R_N lay between cells in the same class, rather than between measurements on the same cell. Although the HRP electrodes demonstrated higher noise levels, the reproducibility was reasonable, as judged by the generally good fit of the regression lines ($R > 0.95$ for all lines) and the small standard deviation around the slope. Also, these results are within the range of values reported for similar neurons (Andersen et al., 1980; Barnes and McNaughton, 1980; Brown et al., 1981*a*; Durand et al., 1983; Schwartzkroin, 1975; Wong and Prince, 1981).

Fig. 3 *A* illustrates the "peeling" procedure used to extract the shorter time constant. The mean time constant values (τ_0) for each cell class in Table II were not distinguishable and averaged overall 17.1 ± 6.67 ms. The time constant ratios (Table II, "Observed") also were not significantly different between the three cell types. This parameter averaged 7.54 ± 3.32 for the three classes combined. The time constant values (Fig. 3, Table II) demonstrated a small standard deviation (1.5% coefficient of variation), which indicates that most of the variance was between cells rather than between measurements. Thus, the electrodes contributed only a small degree of uncertainty to either the R_N or τ_i measurements. Additionally, both the τ_0 and τ_1 values were within the range of other reports for hippocampal neurons (Barnes and McNaughton, 1980; Brown et al., 1981*a*; Durand et al., 1983; Johnston, 1981).

The physiological values for the dendrite to soma conductance ratio (ρ) were similar between the three classes

TABLE I
NEURON ELECTRICAL PARAMETERS*

Hippocampal cell type	R_N‡	Total§ cell area	Membrane‖ resistivity		Average terminating¶ electrotonic distance ($\bar{X}$)
			$\tilde{Y}_t^* = 0$	$\tilde{Y}_t^* = 1$	
	MΩ	*10^{-5} cm²*	*$10^3\Omega \cdot cm^2$*	*$10^3\Omega \cdot cm^2$*	*length constants*
CA1 pyramids					
1/30/3	33.6 ± 1.42	25.3	6.61	14.21	0.57
3/9/1	42.7 ± 0.72	24.6	7.80	13.85	0.53
1/31/2	27.4 ± 0.60	16.3	3.37	6.96	0.84
2/7/3	16.4 ± 0.33	31.3	3.64	5.31	0.83
Mean ± SD	30.0 ± 11.0	24.4 ± 6.2	5.36 ± 2.19	10.08 ± 4.61	0.69 ± 0.17
Dentate granule cells					
11/12/1	63.9 ± 0.77	12.8	4.78	5.40	1.09
11/13/2	46.6 ± 1.34	11.2	3.41	5.71	1.10
2/5/1	49.5 ± 1.21	10.4	3.77	4.26	0.86
2/5/3	53.8 ± 1.35	8.0	2.68	2.95	1.02
Mean ± SD	53.5 ± 7.57	10.6 ± 2.0	3.66 ± 0.87	4.58 ± 1.25	1.02 ± 0.11
CA3 pyramids					
9/19/2	38.6 ± 1.05	26.6	9.14	21.93	0.34
10/15/2	27.6 ± 1.13	65.6	13.74	30.08	0.64
1/26/2	41.0 ± 0.72	57.0	15.99	21.47	0.81
1/26/5	41.3 ± 0.86	39.1	11.90	19.09	0.64
Mean ± SD	37.1 ± 6.46	47.1 ± 17.6	12.69 ± 2.90	23.14 ± 4.79	0.61 ± 0.20
Overall average	40.2 ± 12.85	27.4 ± 18.5	7.24 ± 4.54	12.6 ± 8.87	0.77 ± 0.24

*Group averages are mean ± SD. The group means were significantly different for each of these five parameters, at the $P = 0.01$ level, by an analysis of variance test.

‡R_N is the measured input resistance at the soma of each neuron, which was derived from the slope of a regression line, as in Fig. 3 *B*. The standard deviation given was also derived from the standard deviation of the slope coefficient. All correlation coefficients were $r > 0.95$.

§The total cell area includes the area of both dendritic spines and dendritic branches in the calculations (as in Fig. 2 *A*).

‖$\tilde{Y}_t^* = 0$ denotes a sealed-end assumption at terminals and $\tilde{Y}_t^* = 1$ indicates an infinite cable termination (see text).

¶This value, $\bar{X}$, represents the mean electrotonic distance value for all terminating branches, from the soma outward, assuming $\tilde{Y}_t^* = 0$.

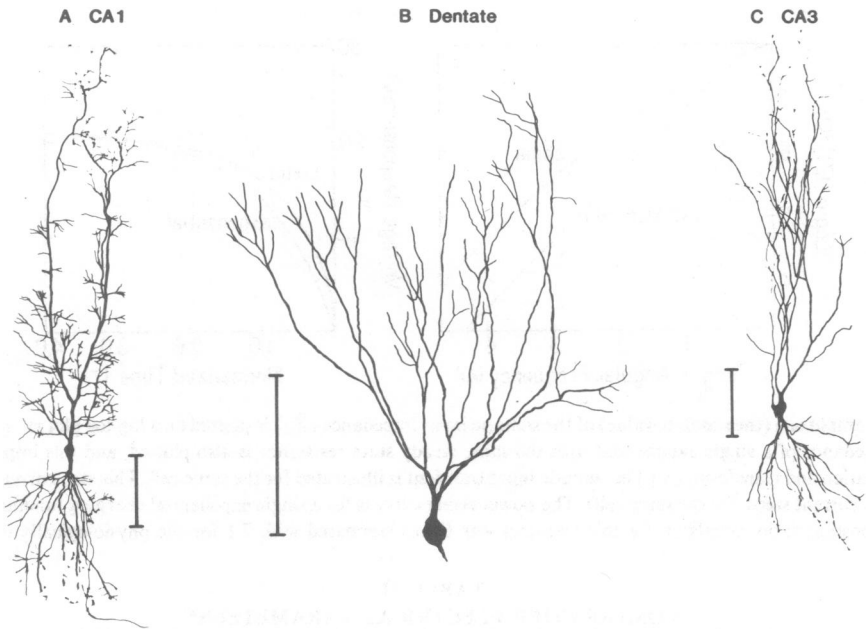

FIGURE 4 (*A*) A camera lucida tracing of a CA1 pyramidal cell, with the apical dendrite and the hippocampal fissure oriented upward and the fimbria below. The scale represents 100 μm. The axon courses downward into the alveus. (*B*) A dentate granule neuron from the upper blade, with the ends of the dendrites just reaching the hippocampal fissure. The axon courses out of the lower part of the soma, toward the hilar region. The scale is again 100 μm. (*C*) A CA3 pyramidal cell, located close to the CA4 region, in the curve of the hippocampal fissure. The apical dendrites point upward in the illustration, while the axon and beginning of a Schaffer collateral course downward and toward the CA1 region. The scale represents 100 μm.

and averaged overall 2.54 ± 1.39, which is somewhat higher than previously reported (1.4 ± 0.55, Brown et al., 1981*a*). The equivalent cylinder L values (Table II, "Observed") did not differ significantly among the three classes. L averaged 0.91 ± 0.23 length constants. This value also appears close to other reported estimates (0.92 ± 0.27, Brown et al., 1981*a*; 1.05 ± 0.22, Durand et al., 1983; 0.9, Johnston, 1981). Thus, aside from the question of the validity of the equivalent cylinder model for these neurons (see Discussion), the present values lie very near other reported equivalent cylinder values.

Anatomical Findings

An example of the dendritic structure of each of the three neuron classes is presented in Fig. 4. The quantitative comparison of total surface area (Table I) demonstrates the large size differences between the cell types. The addition of dendritic spines more than doubled the average cell surface area, increasing it by a factor of 2.19. The HRP-stained neurons revealed excellent anatomical detail, including a profusion of dendritic spines and small dendritic branches by both light and electron microscopy. The anatomical features of these HRP-injected hippocampal neurons were comparable to those described with either Golgi or HRP stains (Durand et al., 1983; Lorente de No, 1934; Minkwitz, 1976; Stansfield and Cowan, 1979; Turner and Schwartzkroin, 1980, 1983; Wenzel et al., 1981).

Specific Membrane Resistivity and Electrotonic Distance

The values for specific membrane resistance (R_m) are presented in Table I. The R_m estimates were significantly different between the regions for each $\tilde{Y}_t^*$ assumption. The R_m values ranged higher than the motoneuron estimates (~2,000–2,700 $\Omega \cdot cm^2$) suggested by Barrett and Crill (1974*a*) and Lux and Schubert (1975). However, the present range of R_m (3.66–23.1 × 10^3 $\Omega \cdot cm^2$) encompassed the values derived for vertebrate retinal cells (Lam and Johnston, 1981) and dorsal root ganglion cells (Brown et al., 1981*b*).

Fig. 6 demonstrates histograms of the terminating electrotonic distance (X) from the soma to individual branch endings. These values are for the $\tilde{Y}_t^* = 0$ assumption; the $\tilde{Y}_t^* = 1$ assumption would predict slightly smaller X values. The average X value ($\overline{X}$) is shown as a vertical bar in Fig. 6 and Table I for each cell type. These averages include both apical and basilar dendrites (for the pyramidal cells); the apical dendrites in these cells possessed slightly larger $\overline{X}$ values (~0.8λ). Fig. 6 clearly demonstrates the wide dispersion of X values for all the cells, and in particular the pyramidal cells.

Comparison of Observed and Simulated Transients

Fig. 5 *A* illustrates the frequency response of the soma (amplitude of $\tilde{Z}_N$ vs. frequency) for the cell presented in

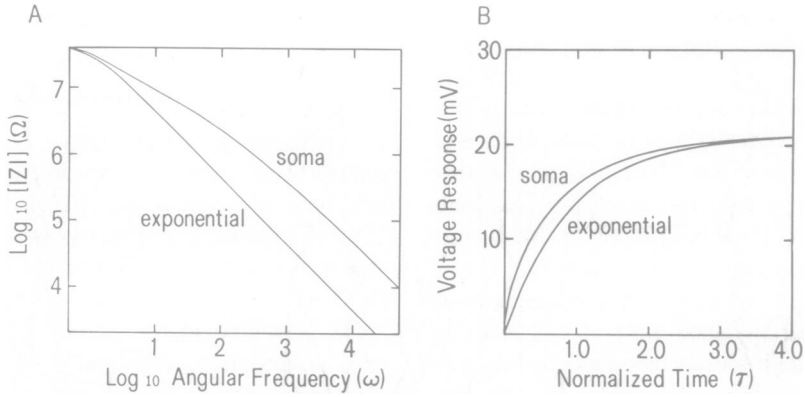

FIGURE 5 (*A*) The amplitude (the absolute value) of the somatic input impedance ($\tilde{Z}_N$) is plotted on a log-log plot vs. angular frequency. For comparison, the impedance of a single exponential with the same steady state resistance is also plotted, and this impedance was used as a control for the calculation and transform. (*B*) The somatic input transient is illustrated for the same cell. This step current input simulates Fig. 3 *A* (both are 0.5-nA current steps, for the same cell). The slower rising curve is for a single exponential charging function, with the same final voltage. The time constant ratio calculated for this transient was 6.3 as compared with 7.1 for the physiologically observed step input in Fig. 3 *A*.

TABLE II
COMPARATIVE ELECTRICAL PARAMETERS*

Hippocampal cell type	Time‡ constant (τ_0)	Time constant ratio§ (τ_0/τ_1)		Equivalent cylinder electrotonic length‖ (*L*, length constant)	
		Observed	Calculated	Observed	Calculated
	ms				
CA1 pyramids					
1/30/3	19.8 ± 0.31	11.06 ± 3.08	5.49 ± 0.63	0.85	0.94
3/9/1	21.1 ± 0.24	7.10 ± 0.70	6.26 ± 0.76	0.90	0.88
1/31/2	18.6 ± 0.38	6.46 ± 0.57	6.10 ± 1.16	1.00	0.85
2/7/3	12.2 ± 0.23	10.47 ± 0.47	5.47 ± 0.66	0.78	0.94
Mean ± SD	17.9 ± 3.95	8.77 ± 2.33	5.83 ± 0.41	0.88 ± 0.09	0.90 ± 0.05
		(t = 2.18,NS)		(t = 0.30,NS)	
Dentate granule cells					
11/12/1	12.6 ± 0.29	3.24 ± 0.65	5.35 ± 0.30	1.45	1.05
11/13/2	9.0 ± 0.24	8.26 ± 2.39	5.39 ± 0.40	0.69	1.00
2/5/1	15.4 ± 0.58	13.62 ± 1.25	6.48 ± 0.57	0.76	0.92
2/5/3	11.8 ± 0.22	7.02 ± 0.74	5.38 ± 0.37	0.93	1.03
Mean ± SD	12.2 ± 2.63	8.04 ± 4.29	5.65 ± 0.55	0.96 ± 0.34	1.00 ± 0.06
		(t = 1.26,NS)		(t = 0.28,NS)	
CA 3 pyramids					
9/19/2	20.7 ± 0.31	10.19 ± 0.82	8.81 ± 1.68	0.85	0.68
10/15/2	34.0 ± 1.23	4.87 ± 0.73	5.45 ± 0.72	1.18	0.90
1/26/2	17.6 ± 0.47	2.50 ± 0.79	5.36 ± 0.52	0.58	0.95
1/26/5	12.2 ± 0.27	5.73 ± 2.00	5.37 ± 0.68	0.97	0.91
Mean ± SD	21.1 ± 9.27	5.83 ± 3.22	6.25 ± 1.71	0.90 ± 0.25	0.86 ± 0.12
		(t = 0.46,NS)		(t = 0.25,NS)	
Overall average	17.1 ± 6.67	7.54 ± 3.32	5.91 ± 1.00	0.91 ± 0.23	0.92 ± 0.10
		(t = 1.85,NS)		(t = 0.13,NS)	

*Individual values are mean ± SD, as are the group averages. The group means were not significantly different for each parameter, using an analysis of variance test (at a level of P = 0.05).

‡The individual SD values for each time constant value were calculated from the standard deviation of the regression slope parameter.

§The "observed" time constant ratios were derived from the physiological transients and the "calculated" values were from the simulated transients. The SD values for both were derived from the 95% confidence limits around the ratio of τ_0/τ_1, derived from the individual SD values for τ_0 and τ_1. The t values in parentheses show the paired comparison of both the individual groups and the overall average, for identity of means. *NS* implies that the null hypotheses (identity of the means) could not be rejected.

‖"Observed" values were derived from the physiological transients and "calculated" values were from the segmental model transients.

Fig. 4 *A*, in addition to a control exponential decay. Fig. 5 *B* demonstrates the somatic voltage transient generated by the segmental cable model for this cell, in response to a step current input. The control transient in this figure was shown to possess a single time constant by the Discrete program analysis (Provencher, 1976). The cell response demonstrated two exponential decays, with a time constant ratio of 6.26 ± 0.76. This step transient was compared with the physiologically observed voltage response in the same cell (Fig. 3 *A*), which had a measured time constant ratio of 7.10 ± 0.70. There were no significant differences (using a paired *t* test; Table II) between the averages of the observed and calculated time constant ratios. Thus, using this index of time constant ratio, the calculated responses adequately approximated the physiologically observed transients.

An additional method was used to evaluate similarity of the observed and calculated transients. This method involved the derivation of electrotonic length (L) and the dendrite to soma conductance ratio (ρ) for both sets of transients (Table II). The equivalent cylinder L values were derived from both the time constant ratio and the τ_i intercepts, so this is a more stringent test of similarity than the comparison of the τ_0/τ_1 ratio alone. The equivalent cylinder assumption was not required for the detailed segmental model, and the L values were used only for comparison of the charging transients. The observed and calculated L values did not differ significantly (Table II), either within or between neuron classes, by the paired *t* test. This agreement also indicates that the observed and calculated transients were reasonably similar (within 5%) at this one site, the soma.

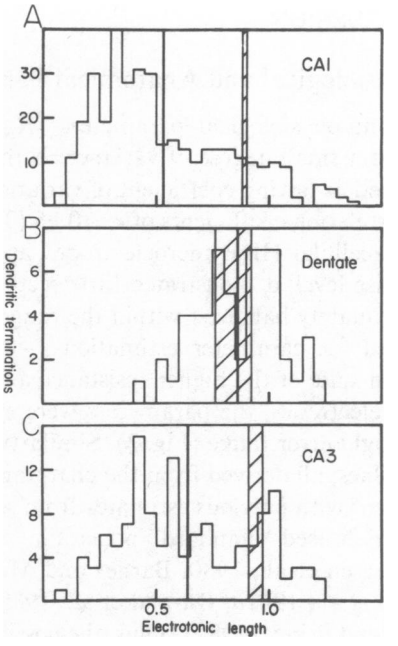

FIGURE 6 (*A*) A plot of the electrotonic distance to all individual dendritic terminations for the CA1 pyramidal cell illustrated in Fig. 4 *A*. The narrow bars with the hatching between indicate the two L values derived from the time constant ratios (for the physiologically observed and calculated transients). The vertical bar to the left is the mean of the anatomically derived terminations ($\overline{X}$), which includes the basilar dendritic tree. (*B*) Same form of plot, but for the dentate granule neuron illustrated in Fig. 4 *B*. The $\overline{X}$ and two L values coincide in this representative neuron. (*C*) This illustrates the $\overline{X}$ and L values for the CA3 pyramidal cell shown in Fig. 4 *C*. Like the CA1 pyramidal cell in *A*, the anatomically derived mean (left-most bar) is lower than the L values predicted by either the observed or calculated transients.

Comparison of Neuron Models

Fig. 6 demonstrates a comparison of the equivalent cylinder L parameter with the $\overline{X}$ values. The dentate granule neurons demonstrated the greatest consistency between the three estimates of electrotonic length ($\overline{X}$, L observed, and L calculated). The dendritic terminations for the representative dentate neuron (Fig. 6 *B*) clustered closely around the three estimates. The coincidence of the two L values with the $\overline{X}$ value and the symmetrical distribution of the terminals around $\overline{X}$ indicates that this unipolar neuron may be adequately represented by an equivalent cylinder model. This conclusion has been reached on other grounds by Turner and Schwartzkroin (1983) and Durand et al. (1983). Certainly, however, there is a relatively wide dispersion of terminals even in the dentate granule neurons. Thus, even these cells may not be well fitted by an equivalent cylinder model neuron for the purpose of evaluating dendritic inputs.

The pyramidal cells consistently demonstrated a divergence of electrotonic length estimates (Fig. 6, *A* and *C*). The two L estimates lay close together, but the $\overline{X}$ value was always smaller. The histogram of terminations for the pyramidal neurons (CA1 and CA3) included both basilar and apical dendritic peaks. Because of the two peaks and the wide dispersion of terminals, the pyramidal cells do not appear to be well approximated (anatomically) by a lumped soma and a single equivalent cylinder. This conclusion has also been reached in earlier studies (Turner and Schwartzkroin, 1980, 1983). These neurons may be more reasonably portrayed by a lumped soma and two unequal (or tapered) equivalent cylinders (Rall, 1977).

Both the single equivalent cylinder model (Brown et al., 1981*a*; Durand et al., 1983) and the present segmental model appear to adequately simulate the observed charging transients in the hippocampal neurons. Thus, the physiological evaluation of somatic responses alone may not be sufficient to decide on the appropriateness of either model for these neurons. Further data may be required, perhaps from an analysis of transients at a site separate from the soma or from an integration of the anatomical evidence (Fig. 6) with the physiological transients. The detailed segmental model appears much more appropriate for dendritic inputs, but either model appears to be adequate to simulate somatic inputs.

DISCUSSION

Physiological and Anatomical Parameters

The important physiological parameters (R_N, τ_i, τ_0/τ_1) demonstrated a small degree of variance: both R_N and τ_0 were measured as having coefficient of variation values of <2% and correlation coefficients of $r > 0.95$ (Tables I and II). The intracellular HRP microelectrodes, apart from an increased noise level, demonstrated little rectification and could be adequately balanced within the range of current injection used for parameter estimation (−0.1 to −0.5 nA). Thus, in spite of the higher resistance and increased noise of the electrodes, the parameters were estimated to lie within a tight error range (Fig. 3). Similarly, R_N, τ_0, τ_1, and the L values, all derived from the charging transients, were consistent with previous estimates from several studies, all of which used "standard" potassium acetate electrodes (Andersen et al., 1980; Barnes and McNaughton, 1980; Brown et al., 1981*a*; Durand et al., 1983; Johnston, 1981; Wong and Prince, 1981). Thus, the possible errors in parameter estimation caused by the HRP electrodes were limited to a small range. This small range of error is considerably less than the variability between cells (Tables I and II).

The visualization of neuronal structure was excellent with an intracellular HRP injection, according to both qualitative and quantitative criteria (Durand et al., 1983; Turner and Schwartzkroin, 1983; Wilson et al., 1983). Electron microscopy of specimens has revealed complete staining of both fine dendritic terminals and dendritic spines (Kunkel, D., D.A. Turner, L. E. Westrum, unpublished observations; Wilson et al., 1983). Compared with the classic standard, Golgi staining, significantly more neuron branches and also smaller branches were revealed by the HRP. There was also little difference between staining revealed by Lucifer Yellow and HRP for hippocampal neurons (Knowles, W. D., D. A. Turner, and P. A. Schwartzkroin, unpublished observations). Thus, HRP-injected neurons appear to be good estimators of total neuronal morphology.

Segmental Cable Model Assumptions

The cable model assumes that the neuronal membrane is adequately represented by a passive network of resistances and capacitances. Applications of this model should thus be restricted to small linear (passive) voltage excursions around the resting potential. In hippocampal neurons, considerable rectification has been observed in both the hyperpolarizing and depolarizing directions (Barnes and McNaughton, 1980; Brown et al., 1981*a*; Johnston, 1981; Schwartzkroin, 1975; Wong and Prince, 1981). However, the passive membrane assumption appeared to be adequately satisfied for the small voltage excursions of 15–20 mV in this study, as evidenced by Fig. 3 *B*.

Another assumption regarding the neuronal membrane is that the specific resistance and capacitance parameters are uniform over the entire surface. Iansek and Redman (1973) and Durand et al. (1983) described evidence that there might be a difference (by a factor of 3) between somatic and dendritic membrane resistance. Barrett and Crill (1974 *a*) also could not disprove this possibility. There are reasons to suspect such nonuniformity of membrane resistivity. These include a poor seal around an intrasomatic electrode, damage caused by the electrode, and tonic inhibitory inputs to the soma. However, the present segmental calculations appear to adequately simulate the observed charging transients without this complicating feature. Thus, there is no convincing reason at present to assume a differential R_m value between soma and dendrites. Such a difference certainly remains a possibility, however, and could easily be accommodated in the segmental model calculations, if required.

Considerable uncertainty may be associated with the anatomic differentiation of somatic from dendritic membrane in these hippocampal cells. The physiologically derived value for ρ is really a distinction of the "isopotential" conductance around the electrode from the dendrite or nonisopotential conductance (Brown et al., 1981*a*). This value may have little correlation (at least for hippocampal neurons) with any anatomic delimitation of soma. The physiological values (0.6–3.5) are much smaller in these neurons than those derived anatomically (6–18), which suggests that the isopotential region around the electrode may be considerably larger than the anatomic soma. The assumption of a lumped, isopotential soma admittance in the segmental model certainly seems well justified from the physiological data.

The neglect of the extracellular resistivity remains a difficult postulate to assess for the dense neuropil of the central nervous system. The sum of the intracellular (r_i) and extracellular (r_e) resistivity is the important factor in calculating the length constant (Rall, 1977). It is unclear how significant this parameter is in a preparation such as the in vitro slice, where there is little spontaneous activity under normal resting conditions. In this resting state, the in vitro central nervous system extracellular space may approach infinite conductivity. Thus, neglect of r_e may not lead to significant error in the calculation of membrane parameters.

Neuron Electrical Parameters

Both the present segmental model and the equivalent cylinder model appear to adequately simulate observed (steady state and transient) physiological characteristics of hippocampal somatic penetrations (Brown et al., 1981*a*; Durand et al., 1983; Johnston, 1981; Johnston and Brown, 1983). However, these two models are distinct from each other in that the present segmental model does not assume that a neuron can be represented by an equivalent cylinder and lumped soma (Rall, 1959, 1969, 1977). Anatomical evidence indicates that hippocampal neurons, particularly

pyramidal cells, are only poorly approximated by the equivalent cylinder model (Turner and Schwartzkroin, 1980, 1983). At the most common recording site, the soma, the two models cannot be distinguished physiologically. Theoretically, however, physiological distinction should be possible (Horwitz, 1981; Rall, 1969), but the differences may be subtle. Additional evidence beyond somatic physiologic recordings may be necessary to demarcate the meaning of structural deviations from the equivalent cylinder model. Either the anatomical data presented above or recording from additional neuronal sites may provide such evidence. For sites other than the soma, the detailed segmental approach appears to be much more appropriate for these neurons, according to anatomical criteria.

Recent work by Segev and Rall (1983) indicates that the single L value should lie between the apical dendritic value ($\overline{X}_a \sim 0.8\lambda$) and the sum of the apical and basilar dendrites ($\overline{X}_b \sim 0.3\lambda$; $\overline{X}_a + \overline{X}_b \sim 1.1\lambda$). The derived L value of 0.91 length constants for these neurons does indeed lie between $\overline{X}_a$ and $\overline{X}_a + \overline{X}_b$. For a unipolar cell, such as the dentate granule neurons, the L values more closely approximate the $\overline{X}$ values (Fig. 6 *B*; Tables I and II). By this criterion, the dentate granule cells do approach an ideal equivalent cylinder model, in spite of the wide distribution of terminations (Fig. 6 *B*; see also Durand et al., 1983).

The average hippocampal electrotonic length of ~0.6–1.0λ contrasts with the generally longer values (1–2λ) derived for spinal neurons (Barrett and Crill, 1974*a*; Iansek and Redman, 1973; Lux and Pollen, 1966; Lux and Schubert, 1975; Rall, 1977), olfactory bulb cells (Mori et al., 1981), and neocortical neurons (Vogt and Gorman, 1982). A wide range of other reported L values has been reviewed by Brown et al. (1981*b*). The electrical implications of these L values have been discussed in regard to motoneurons (Barrett and Crill, 1974*b*; Jack and Redman, 1971) and hippocampal neurons (Traub and Llinas, 1979; Turner and Schwartzkroin, 1980, 1983). However, electrotonic distance does not appear to be the sole determinant of synaptic efficacy. Other factors, such as dendritic input impedances and voltage transfer, may be minimally dependent on the X value for a particular site (Turner and Schwartzkroin, 1983). The issue of synaptic potency and dendritic spine transients will be discussed more fully in the following paper (Turner, 1984) for two classes of hippocampal neurons.

I thank Dr. James Randall for helpful discussions regarding the Fourier transforms, Dr. Per Andersen for his contributions on the significance of this analysis, and Mr. Bruce Piercy for diligently maintaining the computer facilities. I also thank Drs. Wilfred Rall and Maurizio Mirolli for extensive discussion and criticism of the work.

This study was supported by National Institutes of Health Postdoctoral Fellowship (Individual) NS06792, a Veterans Administration Research Service Award, and Minnesota Medical Foundation grant FSW-86-83.

Received for publication 26 July 1983 and in final form 8 February 1984.

REFERENCES

Andersen, P., H. Silfvenius, F. H. Sundberg, and O. Sveen. 1980. A comparison of distal and proximal dendritic synapses on CA1 pyramids in guinea-pig hippocampal slices in vitro. *J. Physiol. (Lond.).* 307:273–299.

Barnes, C. A., and B. L. McNaughton. 1980. Physiological compensation for loss of afferent synapses in rat hippocampal granule cells during senescence. *J. Physiol. (Lond.).* 309:473–485.

Barrett, J. N., and W. E. Crill. 1974 *a*. Specific membrane properties of cat motoneurons. *J. Physiol. (Lond.).* 239:301–324.

Barrett, J. N., and W. E. Crill. 1974 *b*. Influence of dendritic location and membrane properties on the effectiveness of synapses on cat motoneurons. *J. Physiol. (Lond.).* 239:325–345.

Brown, T. H., R. A. Fricke, and D. H. Perkel. 1981*a*. Passive electrical constants in three classes of hippocampal neurons. *J. Neurophysiol. (Bethesda).* 46:812–827.

Brown, T. H., D. H. Perkel, J. C. Norris, and J. H. Peacock. 1981*b*. Electrotonic structure and specific membrane properties of mouse dorsal root ganglion neurons. *J. Neurophysiol. (Bethesda).* 45:1–15.

Durand, D., P. L. Carlen, N. Gurevich, A. Ho, and H. Kunov. 1983. Electrotonic parameters of rat dentate granule cells measured using short current pulses and HRP staining. *J. Neurophysiol. (Bethesda).* 50:1080–1097.

Englisch, H. J., G. Kunz, and J. Wenzel. 1974. Zur Spines-Verteilung an Pyramiden-Neuronen der CA1-Region des Hippocampus der Ratte. *Z. Mikrosk. Anat. Forsch. (Leipz.).* 88:85–102.

Feldman, M. L., and A. Peters. 1979. A technique for estimating total spine numbers on Golgi-impregnated dendrites. *J. Comp. Neurol.* 188:527–542.

Fifkova, E., and C. L. Anderson. 1981. Stimulation-induced changes in dimensions of stalks of dendritic spines in the dentate molecular layer. *Exp. Neurol.* 74:621–627.

Fifkova, E., and A. Van Harreveld. 1977. Long lasting morphological changes in dendritic spines of dentate granule cells following stimulation of the entorhinal area. *J. Neurocytol.* 6:211–230.

Horwitz, B. 1981. An analytical method for investigating transient potentials in neurons with branching trees. *Biophys. J.* 36:155–192.

Iansek, R., and S. J. Redman. 1973. An analysis of the cable properties of spinal motoneurons using a brief intracellular current pulse. *J. Physiol. (Lond.).* 234:613–636.

Jack, J. J. B., and S. J. Redman. 1971. An electrical description of the motoneurone, and its application to the analysis of synaptic potentials. *J. Physiol. (Lond.).* 215:321–352.

Johnston, D. 1981. Passive cable properties of hippocampal CA3 pyramidal neurons. *Cell. Mol. Neurobiol.* 1:41–55.

Johnston, D., and T. H. Brown. 1983. Interpretation of voltage-clamp measurements in hippocampal neurons. *J. Neurophysiol. (Bethesda).* 50:464–486.

Koch, C., T. Poggio, and V. Torres. 1982. Retinal ganglion cells: a functional interpretation of dendritic morphology. *Philos. Trans. R. Soc. Lond. B Biol. Sci.* 298:227–264.

Lam, D. M., and D. Johnston. 1981. Active and passive membrane properties of isolated horizontal cells from the catfish retina. *Nature (Lond.).* 292:451–453.

Lee, K. S., F. Schottler, M. Oliver, and G. Lynch. 1980. Brief bursts of high-frequency stimulation produce two types of structural change in rat hippocampus. *J. Neurophysiol. (Bethesda).* 44:247–258.

Lorente de No, R. 1934. Studies on the structure of the cerebral cortex. II. Continuation of the study of the ammonic system. *J. Psychol. Neurol.* 46:225–242.

Lux, H. D., and D. A. Pollen. 1966. Electrical constants of neurons in the motor cortex of the cat. *J. Neurophysiol. (Bethesda).* 29:207–220.

Lux, H. D., and P. S. Schubert. 1975. Some aspects of the electroanatomy of dendrites. *Adv. Neurol.* 12:29–44.

Meyer, G., and R. Ferres-Torres. 1978. Quantitative altersabhangige Variation der dendriten Spines in Hippocampus (CA1, CA3 und Fascia Dentata) der Albminomaus. *J. Hirnforsch.* 19:371–378.

Minkwitz, H.-G. 1976. Zur Entwicklung der Neuronenstruktur des Hippocampus während der prä- und postnatalen Ontogenese der Albinoratte. I. Mitteilung: Neurohistologische Darstellung der Entwicklung von langaxoniger Neurone aus der Regionen CA3 and CA4. *J. Hirnforsch.* 17:213–231.

Mori, K., M. C. Nowycky, and G. M. Shepherd. 1981. Electrophysiological analysis of mitral cells in the isolated turtle olfactory bulb. *J. Physiol. (Lond.).* 314:281–294.

Norman, R. S. 1972. Cable theory for finite length dendritic cylinders with initial and boundary conditions. *Biophys. J.* 12:25–45.

Provencher, S. W. 1976. A Fourier method for the analysis of exponential decay curves. *Biophys. J.* 16:27–41.

Rall, W. 1959. Branching dendritic trees and motoneuron membrane resistivity. *Exp. Neurol.* 1:491–527.

Rall, W. 1969. Time constants and electrotonic length of membrane cylinders and neurons. *Biophys. J.* 9:1483–1508.

Rall, W. 1974. Dendritic spines, synaptic potency and neuronal plasticity. *In* Cellular Mechanisms Subserving Changes in Neuronal Activity. C. O. Woody, K. S. Brown, T. J. Crown, and J. D. Knispel, editors. Brain Information Service, Los Angeles. 13–21.

Rall, W. 1977. Core conductor theory and cable properties of neurons. *In* Handbook of Physiology, Section I: The Nervous System. E. R. Kandel, editor. Williams & Wilkins Co., Baltimore, 39–97.

Rinzel, J., and W. Rall. 1974. Transient response in a dendritic neuron model for current injected at one branch. *Biophys. J.* 14:759–790.

Scheibel, M. E., and A. B. Scheibel. 1968. On the nature of dendritic spines-report of a workshop. *Commun. Behav. Biol. Part A Orig. Artic.* 1:231–265.

Schwartzkroin, P. A. 1975. Characteristics of CA1 neurons recorded intracellularly in the hippocampal "in vitro" slice preparation. *Brain Res.* 85:423–436.

Segev, I., and W. Rall. 1983. Theoretical analysis of neuron models with dendrites of unequal electrical lengths. *Neurosci. Abstr.* 9:341.

Stansfield, B. B., and W. M. Cowan. 1979. The morphology of the hippocampus and dentate gyrus in normal and reeler mice. *J. Comp. Neurol.* 185:393–422.

Traub, R. D., and R. Llinas. 1979. Hippocampal pyramidal cells: significance of dendritic ionic conductances for neuronal function and epileptogenesis. *J. Neurophysiol. (Bethesda).* 42:476–496.

Turner, D. A. 1982. Soma and dendritic spine transients in intracellularly-stained hippocampal neurons. *Neurosci. Abstr.* 8:945.

Turner, D. A. 1984. Conductance transients onto dendritic spines in a segmental cable model of hippocampal neurons. *Biophys. J.* 46:000–000.

Turner, D. A., and P. A. Schwartzkroin. 1980. Steady-state electrotonic analysis of intracellularly-stained hippocampal neurons. *J. Neurophysiol. (Bethesda).* 44:184–199.

Turner, D. A., and P. A. Schwartzkroin. 1983. Electrical characteristics of dendrites and dendritic spines in intracellularly-stained CA3 and dentate hippocampal neurons. *J. Neurosci.* 3:2381–2394.

Valverde, F., and A. Ruiz-Marcos. 1969. Dendritic spines in the visual cortex of the mouse: introduction to a mathematical model. *Exp. Brain Res.* 8:269–283.

Vogt, A. B., and A. L. F. Gorman. 1982. Responses of cortical neurons to stimulation of the corpus callosum in vitro. *J. Neurophysiol. (Bethesda).* 48:1257–1273.

Wenzel, J., W. Kirsche, G. Kune, T. Neumann, H. Wenzel, and E. Winkelman. 1973. Licht- und electronen mikroskopische Untersuchungen uber die dendriten Spines an Pyramiden-Neuronen des Hippocampus (CA1) bei der Ratte. *J. Hirnforsch.* 13:387–408.

Wenzel, J., G. Stender, and G. Duwe. 1981. The development of the neuronal structure of the fascia dentata of the rat. Neurohistologic, morphometric, ultrastructural and experimental investigations. *J. Hirnforsch.* 22:629–683.

Westrum, L. E., and T. W. Blackstad. 1962. An electron microscopic study of the stratum radiatum of the rat hippocampus (CA1) with particular emphasis on synaptology. *J. Comp. Neurol.* 11:281–309.

Wilson, C. J., P. M. Groves, S. T. Kitai, and J. L. Linder. 1983. Three-dimensional structure of dendritic spines in the rat neostriatum. *J. Neurosci.* 3:383–398.

Wong, R. K. S., and D. A. Prince. 1981. Afterpotential generation in hippocampal pyramidal cells. *J. Neurophysiol. (Bethesda).* 45:86–97.